Digital Signal Processing 80 (2018) 57–69

Contents lists available at ScienceDirect

Digital Signal Processing

www.elsevier.com/locate/dsp

Waveform design for communicating radar systems using Fractional Fourier Transform

Domenico Gaglione [a,*], Carmine Clemente [b], Christos V. Ilioudis [b], Adriano Rosario Persico [b], Ian K. Proudler [c], John J. Soraghan [b], Alfonso Farina [d]

[a] NATO STO Centre for Maritime Research and Experimentation (CMRE), La Spezia, Italy
[b] Centre for Signal and Image Processing (CeSIP), University of Strathclyde, Glasgow, UK
[c] School of Electronic, Electrical and Systems Engineering, Loughborough University, Leicestershire, UK
[d] Professional Consultant, Rome, Italy

ARTICLE INFO

Article history:
Available online 17 May 2018

Keywords:
Joint radar–communication system
Fractional Fourier Transform (FrFT)
Waveform design
Software Defined Radio (SDR)

ABSTRACT

A novel waveform design technique for enabling a communication channel within a pulse radar is presented. The proposed waveform is composed of quasi-orthogonal chirp sub-carriers generated by means of the Fractional Fourier Transform (FrFT), with the aim of preserving the radar performance of a typical Linear Frequency Modulated (LFM) pulse while embedding data to be sent to a cooperative system. Waveform generation and demodulation are described, together with techniques aimed at optimising the design parameters and mitigating the Inter-Carrier Interference (ICI) caused by the quasi-orthogonality of the chirp sub-carriers. The proposed FrFT based communicating-radar (CoRadar) waveform design is compared with Orthogonal Frequency Division Multiplexing (OFDM) based CoRadar with respect to both radar and communication operations. Radar performance is evaluated through examination of the Ambiguity Function (AF) and by assessing the performance of a standard square law detector. Communication performance is shown in terms of Bit Error Ratio (BER) for different channel conditions. Results demonstrate that the proposed FrFT waveform presents performance close to a LFM pulse in terms of probability of detection and probability of false alarm, in exchange for slightly worse range and Doppler resolution. Furthermore, it is shown to maintain comparable communication performance with respect to the OFDM waveform. Finally, a hardware implementation is described that demonstrates the simultaneous radar and communication capabilities of the proposed system.

1. Introduction

In several applications there is the dual need for a system to perform radar operations while sending data to another cooperative system. Examples are vehicles in an Intelligent Transportation System (ITS) that need to share information in a rapidly changing environment [1]; Synthetic Aperture Radar (SAR) systems that need to share sensed data with ground stations [2]; nodes in a Multiple-Input Multiple-Output (MIMO) radar system for the purposes of surveillance or navigation aid [3]. A straightforward solution to this problem is the use of two actual systems, one performing the radar task and another in charge of data transmission. This can be achieved by enforcing spectral constraints on the radar and the communication signals [4–6], or allowing the radar waveform to dynamically adapt to the presence of communication systems [7], and vice-versa [8]. However, the employment of two separate systems to accomplish the radar and the communication operations may be not efficient, since both of them require their own power, hardware and frequency resources. This is in contrast with the low-SWaP (Size, Weight and Power consumption) requirements that an increasing number of applications demands together with the challenge of spectrum congestion [9].

The idea of designing a system capable of simultaneously performing the radar and the communication tasks while sharing hardware, power and bandwidth resources, was first introduced in [10]. Nowadays, the joint radar–communication (CoRadar) system concept is becoming ever more appealing to the radar community, and it is seen as a potential feature in future radar systems [11]. A block diagram of a CoRadar system is depicted in Fig. 1. The illustration highlights the functions that are exclusive to the radar and to the communication operations, in green and red, respectively, and the blocks that are shared, in light blue. Source encoder, channel encoder and modulator, typical functions of a communication system [12], pre-process the data that needs to be embedded

* Corresponding author.
E-mail address: domenico.gaglione@cmre.nato.int (D. Gaglione).

https://doi.org/10.1016/j.dsp.2018.05.002

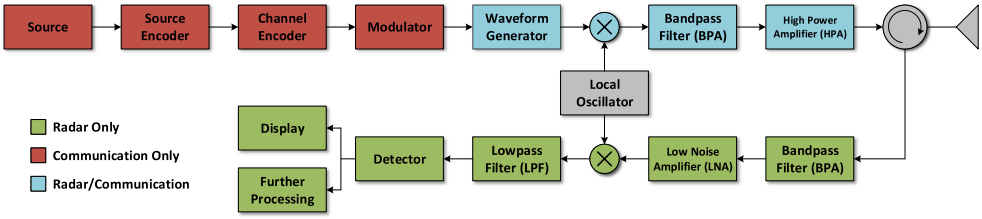

Fig. 1. General working principle of a communicating radar (CoRadar) system. Blocks that are exclusive for either radar or communication operations are highlighted in green and red, respectively. Blocks that are shared between the two tasks are highlighted in light blue (for interpretation of the colours in the figure, the reader is referred to the web version of this article).

in the transmitted waveform. This is then generated by taking into account the radar requirements, such as range and Doppler resolutions, desired Side Lobe Levels (SLLs), etc. Finally, the signal is sent to a Radio Frequency (RF) front-end. The received waveform, instead, is viewed as a target reflected radar signal, therefore it undergoes standard radar processing.

The radar and the communication signals can be independently generated and then merged by efficiently allocating their spectra, as proposed in [13] and in [14], or data can be directly embedded into the transmitted radar waveform [15]. The embedding of the data can be achieved using a time-duplexing scheme, in which the transmitted signal is formed by alternating a radar and a data-modulated waveform. Following this idea, in [16] long-range pulses of a Senrad radar [17], originally time-duplexed with short-range pulses, were replaced by communication signals carrying 600 bits each. The system so obtained was able to transmit with a data rate of 900 b/s, giving up, however, on the long-range function of the radar. Similarly, a short-range CoRadar for automotive application was described in [18]. The transmitted signal comprises a radar cycle, based on a Trapezoidal Frequency Modulated Continuous Waveform (TFMCW), followed by a single frequency carrier modulated by information data using common modulation techniques, such as Phase Shift Keying (PSK). The system was able of sending data at 75 Mb/s, with a Bit Error Ratio (BER) of 10^{-6}, while detecting target at a maximum unambiguous range of 100 m.

A code-duplexing scheme, instead, that exploited the Direct Sequence Code Division Multiple Access (DS-CDMA) technique to avoid mutual interference between radar and communication signals was proposed in [19]. The orthogonality between radar and communication signals was achieved in [20] by using an up- and a down-chirp. The implementation of such a system was reported in [21]. It operated with a bandwidth of 500 MHz and a Pulse Repetition Frequency (PRF) of 150 kHz, capable of transmitting 1 Mb/s with a BER lower than 10^{-5} at a maximum unambiguous range of 1 km.

Alternative reported methods use either Stepped Frequency Continuous Waveforms (SFCW) [22] or Linear Frequency Modulated (LFM) pulses phase-modulated by Binary PSK (BPSK) [23]. In these cases, the number of symbols per waveform is limited to the square root of the time-bandwidth product. Multi-carrier signals [24], widely used in modern radars for their high time-bandwidth product and flexibility, also represent natural candidates for the implementation of a CoRadar system. The idea was introduced in [25], where the authors combined a co-located MIMO radar with Orthogonal Frequency Division Multiplexing (OFDM) communications by employing a step-frequency technique, achieving a data rate of 386.4 kb/s at a maximum unambiguous range of 74.88 km. A signal processing solution that circumvented the high side-lobes problem that arises when performing usual radar operations on OFDM signals, was presented in [26]. The drawback was the introduction of periodicities in the radar range profile, that limited the unambiguous range of the system, able of transmitting data at 20 Mb/s, to 1650 m [1]. In addition to the problem of high side-lobes, OFDM signals also exhibit high Peak-to-Average Power Ratios (PAPRs) that limit their practical application. This aspect has been widely investigated in communication literature, leading to well-known and widely used techniques such as companding [27] and active constellation extension [28].

CoRadar approaches based on the joint use of waveform diversity and side lobe control have also been recently reported. In [29] a dual-function system based on time-modulated array was proposed, which implemented the radar function in the main lobe while the communication was performed in the side lobe by exploiting the variation of the beam pattern. A similar idea was presented in [30] wherein each orthogonal waveform embedded one information bit, whose value depended on the radiation beam pattern employed. Finally, in [31] the information was embedded in the differential phase between two beamforming weight vectors, which did not affect the radar operation in the main beam.

1.1. Proposed method

As discussed, many of the CoRadar waveform design techniques presented above either are meant for short-range applications, i.e. automotive, or suffer from low data rates. In this paper a novel Fractional Fourier Transform (FrFT) based waveform design method for CoRadar systems [32] is presented and analysed. This technique aims to preserve the radar performance typical of an LFM pulse, while exploiting the quasi-orthogonality of different chirp rates to embed data. Moreover, unlike other approaches, it does not require a phased array antenna, thus not limiting the scope of application. The design of the waveform is driven by the radar requirements, such as the bandwidth and the pulse duration, and, depending on the application, the maximum detectable range can vary from few to hundreds km, while the data rate can be as high as few Mb/s at medium-long distances.

The FrFT has already been successfully employed in radars as waveform design tool for MIMO radar systems [33–36] and cognitive radars [37], for target detection [38] and SAR processing [39, 40], as well as for wireless RF [41] and underwater communication systems [42]. The main contributions of this paper are summarised below:

- description of a novel FrFT based waveform design technique for CoRadar system;
- introduction of optimisation procedures for maximising the throughput of the system;
- assessment of the radar and the communication performance and link budget analysis;
- feasibility demonstration through the implementation of the proposed approach on a Software Defined Radio (SDR) device.

The remainder of the paper is organised as follows. Section 2 introduces the FrFT and the proposed waveform design, while three optimisation procedures are described in Section 3. Section 4 presents the radar and communication performance and Section 5 describes the implementation of a real-time CoRadar system based

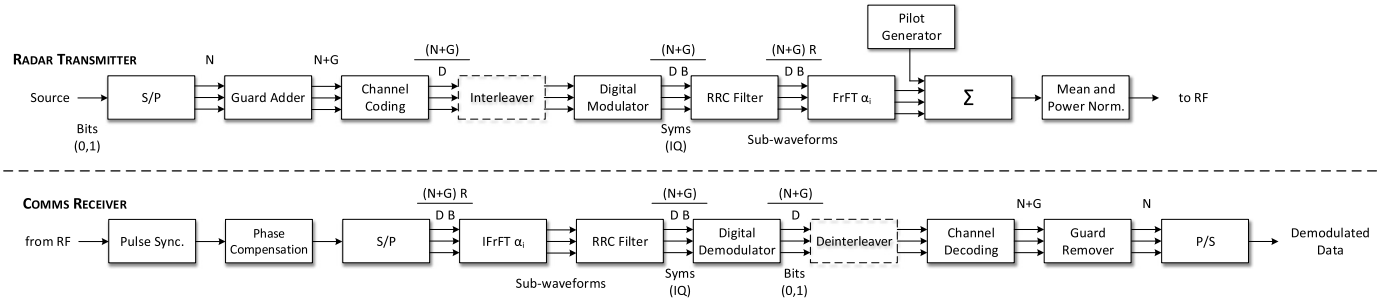

Fig. 2. Block diagram of (top) the FrFT Radar Transmitter, in charge of the waveform generation, and (bottom) the FrFT Communication Receiver, whose task is the demodulation of the received pulses.

on the proposed waveform design. In Section 6 some practical open challenges are reported while Section 7 concludes the paper.

2. FrFT CoRadar system

In this Section, the Fractional Fourier Transform (FrFT) based CoRadar waveform design is presented. It is a multiplexing scheme that uses the FrFT to map the in-phase and quadrature (IQ) symbols of a selected modulation scheme to different chirp, or Linear Frequency Modulated (LFM), sub-carriers with different time-frequency rates. Hereafter, following a brief introduction on the FrFT, the proposed waveform generation and demodulation are described.

2.1. Fractional Fourier Transform (FrFT)

The FrFT belongs to the class of linear Time-Frequency Representations (TFRs), and it was firstly introduced in [43]. It is a generalisation of the ordinary Fourier transform and can be considered as a rotation by an arbitrary angle, ϕ, in the time-frequency plane. Letting $x[u]$ be an arbitrary signal of length U, its α-th order discrete FrFT is defined as [44]:

$$X_\alpha[u] = \sum_{u'=-U/2}^{U/2} K_\alpha[u,u']\,x[u'] \tag{1}$$

where

$$\alpha = \frac{2\phi}{\pi} \tag{2}$$

is the fractional order and $K_\alpha[u,u']$ is the FrFT kernel, defined as [44]:

$$K_\alpha[u,u'] = \begin{cases} A_0 e^{j\pi(u^2+u'^2)\cot\phi} \times & \text{if } \phi \neq m\pi \\ \quad e^{-j\pi 2uu'\csc\phi} & \\ \delta[u-u'] & \text{if } \phi = 2m\pi \\ \delta[u+u'] & \text{if } \phi = 2m\pi+\pi \end{cases} \tag{3}$$

where $A_0 = \frac{e^{j\frac{\phi}{2}}}{\sqrt{j\sin\phi}}$, $\delta(\cdot)$ is the Dirac delta function, $j = \sqrt{-1}$ and $m \in \mathbb{Z}$ is an integer. The FrFT is an invertible linear transform continuous in the angle ϕ, which satisfies the basic conditions for it to be meaningful in the time-frequency plane [45].

2.2. Waveform generation

The waveform design is shown at the top of Fig. 2. The bits to be embedded in the CoRadar pulse are divided into $C-1$ segments of N bits each by the serial-to-parallel (S/P) block, where C is the number of chirp sub-carriers to use. The 0-th order sub-carrier is not used to carry information bits, since it accommodates a pilot waveform used at the communication receiver for synchronisation and phase compensation. Therefore, each pulse contains $N \times (C-1)$ information bits, leading to a final bit rate of $N \times (C-1) \times \mathrm{PRF}$ b/s, where PRF is the Pulse Repetition Frequency.

In each segment, G guard bits are added at the end of the sequence in order to compensate the group delay introduced by the Root Raised Cosine (RRC) filter [46]. Then, a binary block code with code rate D [12] is applied, leading to a coded sequence of $(N+G)/D$ bits, and an interleaver may be used to mitigate the Inter-Carrier Interference (ICI); this solution is discussed in more detail later in the paper. Finally, the digital modulator maps a series of B bits to any of the $M = 2^B$ complex symbols according to the employed modulation scheme (i.e. MPSK). The final sequence is then composed by $U = (N+G) \times R/(D \times B)$ samples, where R is the up-sampling factor of the RRC filter.

The $C-1$ sub-waveforms so obtained, referred to as $x_i[n]$, with $i = 1,\ldots,C-1$, are then mapped, through equation (1), to different chirp sub-carriers uniformly spaced in the time-frequency domain. Note that the FrFT is periodic in ϕ with period 2π, however rotations of ϕ and $\phi+\pi$ produce signals that overlap in the time-frequency plane. For this reason, only angles in the range $[0,\pi)$ are considered, that leads to $\alpha \in [0,2)$. Thus, the uniformly spaced sub-carriers are obtained by choosing the i-th fractional order to be equal to $\alpha_i = i\,\bar{\alpha}$, where $\bar{\alpha} = \frac{2}{C}$. The transmitted waveform is then obtained by adding the chirp modulated sub-waveforms and the pilot waveform, $p[n]$, that is:

$$s_{tx}[n] = p[n] + \sum_{i=1}^{C-1} \sum_{u=-U/2}^{U/2} K_{\alpha_i}[n,u]\,x_i[u] \tag{4}$$

Before sending it to the RF front-end, its mean is removed and the power is normalised such that all the transmitted pulses present the same power.

The spectrogram of a FrFT CoRadar waveform with relatively few sub-carriers ($C = 7$) is shown in Fig. 3 for clarity, although in practice the spectrogram could appear more crowded. The time

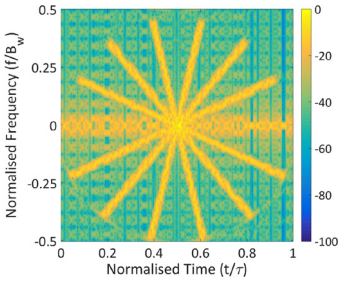

Fig. 3. Spectrogram of a FrFT CoRadar waveform with 7 sub-carriers.

axis is normalised to the length of the CoRadar pulse, τ, while the frequency axis is normalised to its bandwidth:

$$B_w = \frac{U}{\tau} = \frac{N+G}{D\,B}\frac{R}{\tau} \tag{5}$$

2.3. Waveform demodulation

The co-operative communication system that receives the sequence of CoRadar pulses demodulates them and extracts the embedded information. A block diagram of this Comms Receiver is shown in Fig. 2. Once the synchronisation and the phase compensation are performed by exploiting the pilot waveform,[1] the acquired signal, whose length is U samples, is redirected to $C-1$ different IFrFT blocks that perform the inverse FrFT with order α_i. Each sequence is then input of the RRC filter, which also downsamples the sub-waveform by a factor R, and then the digital demodulator that translates the sequence of symbols in a sequence of bits. At this point, a de-interleaver may be placed which performs the inverse operation of the interleaver. Finally, the channel decoding block, which extracts the $N+G$ uncoded bits while performing the error correction, is followed by the guard remover and the P/S blocks, that reconstruct the original stream by combining the N-long bit sequences coming from the $C-1$ different parallel branches.

3. FrFT CoRadar waveform optimisation

In this Section three waveform optimisation procedures are described. The introduction of either a guard time or an interleaver has the objective of minimising the Inter-Carrier Interference (ICI), caused by the overlap of the chirp sub-carriers. Then, for both these methods, a parameters selection process is presented that maximises the data rate while fixing some parameters that meet the radar requirements. Finally, the adaptive duration technique of the sub-waveforms that aims to efficiently occupy the available bandwidth is introduced.

3.1. ICI mitigation

Due to the nature of chirps, when more than one sub-carrier is used there is an overlapping area with centre at the zero frequency and half duration of the pulse that produces ICI. In this Section two ICI mitigation approaches are proposed for the developed waveform design, namely guard time and interleaver.

3.1.1. Guard time

In order to avoid data loss, the time-frequency region affected by ICI is not used for the transmission of bits of information but carries guard bits instead. This can be achieved by slightly modifying the guard adder block in Fig. 2, such that it adds both G_2 bits in the middle of the sequence to mitigate the ICI and G_1 bits at the end in order to compensate the group delay introduced by the RRC filter. This leads to an overall guard band width of $G = G_1 + G_2$. To compute the amount of guard bits G_2 needed to mitigate the ICI, let us introduce the normalised guard time T_G, equal to:

$$T_G = \rho\, Q \tag{6}$$

where $\rho \in (0, 1]$ and Q is a measure of the sub-carriers overlap, graphically represented by the diameter of the red circle in Fig. 4. The value Q depends on the inter-carrier separation angle $\psi = \phi_{i+1} - \phi_i = \pi/C, \forall i = 0, \ldots, C-2$, with ϕ_i be the rotation angle of the i-th chirp sub-carrier. Through geometrical considerations, Q is equal to:

$$Q = \frac{B_{w,sub}}{B_w}\csc\left(\frac{\pi}{2C}\right) \tag{7}$$

where $\csc(\cdot)$ indicates the cosecant of the argument. The term $B_{w,sub}$ is the bandwidth of each sub-waveform, equal to:

$$B_{w,sub} = \frac{N+G_1+G_2}{D\,B}\frac{\beta+1}{\tau} \tag{8}$$

where β is the RRC roll-off coefficient. The result obtained in (7) is graphically explained by Fig. 5, which depicts the same setup reported in Fig. 4 with either (a) double the number of sub-carriers or (b) double the bandwidth of each sub-waveform. It is intuitively clear how Q increases, namely the ICI gets worse, as the number of sub-carriers and the bandwidth of each sub-waveform increase, with respect to the original case identified by the red dashed circle. The guard time T_G finally translates to a guard band width of G_2 bits given by:

$$G_2 = \left\lfloor (N+G_1)\frac{T_G}{1-T_G} \right\rfloor = \left\lfloor (N+G_1)\frac{\rho Q}{1-\rho Q} \right\rfloor \tag{9}$$

where the operator $\lfloor\cdot\rfloor$ gives the largest integer not greater than the argument.

3.1.2. Interleaver

The second approach to mitigate the ICI is the use of an interleaver. As shown in Fig. 4, the interference is localised around the centre of rotation of the waveform. This means that it generates a burst of errors, affecting a small group of bits that can be dealt with the use of a suitable interleaving technique [47].

3.2. Parameters selection

In the proposed CoRadar system the radar task is given priority over the communication one. For this reason the proposed parameters selection process starts from the pulse's bandwidth, B_w,

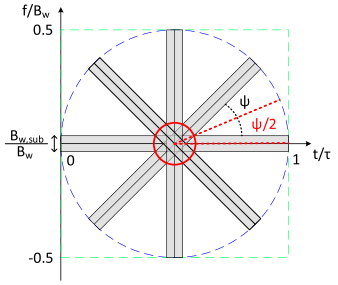

Fig. 4. Waveform optimisation: representation of the region affected by Inter-Carrier Interference (ICI).

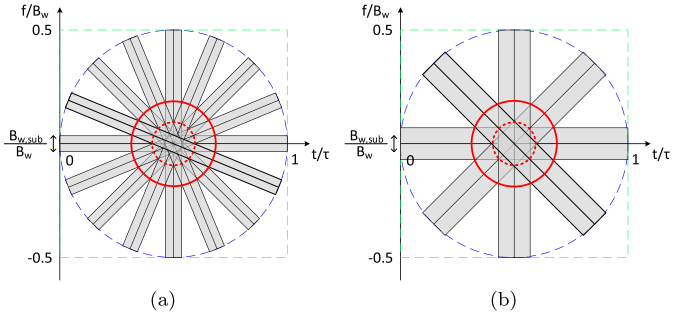

Fig. 5. Graphical representation of the increase of the ICI as (a) the number of sub-carriers or (b) the bandwidth of each sub-waveform increase, with respect to Fig. 4.

[1] Note that the alignment with the received signal on a sample basis is needed to perform the inverse FrFT.

and duration, τ, that account for some radar requirements such as range and Doppler resolution and minimum detectable range, and aims to derive the other parameters in order to maximise the bit rate. Assuming that the number of bits per symbol, B, the code rate, D, and the number of guard bits, G_1, are fixed, the following procedure derives the number of sub-carriers, C, of bits per sub-carriers, N, and the up-sampling factor, R. The process differs depending on the ICI mitigation technique used.

3.2.1. Guard time

The number of samples per waveform, U, is bounded by the time-bandwidth product as follows (see equation (5)):

$$\tau\, B_w \geqslant (N + G_1 + G_2)\, \frac{R}{D\, B} = \frac{N + G_1}{(1 - \rho\, Q)}\, \frac{R}{D\, B} \tag{10}$$

where the last analytical step uses (9). By rewriting Q in (7) by means of (5) and (8) as:

$$Q = \frac{\beta + 1}{R} \csc\left(\frac{\pi}{2C}\right) \tag{11}$$

and substituting (11) into (10), a quadratic inequality in R can be obtained, such that $R_{\min} \leqslant R \leqslant R_{\max}$, which admits real solutions only if the following condition is met:

$$C\,(N) \leqslant \frac{\pi}{2} \frac{1}{\sin^{-1}\left(4 \dfrac{N + G_1}{D\, B} \dfrac{\rho\,(\beta + 1)}{\tau\, B_w}\right)} \tag{12}$$

where the dependency of C on N is highlighted for clarity. Thus the maximum data rate occurs when:

$$C\,(N) = \left\lfloor \frac{\pi}{2} \frac{1}{\sin^{-1}\left(4 \dfrac{N + G_1}{D\, B} \dfrac{\rho\,(\beta + 1)}{\tau\, B_w}\right)} \right\rfloor \tag{13}$$

Recalling that the bit rate is proportional to $N \times (C - 1)$, the parameters selection can be achieved by following this iterative procedure:

1. Find an N such that:

$$\max_N [N \times (C\,(N) - 1)] \quad \text{subject to} \quad N \in \mathbb{N} \tag{14}$$

   while fixing ρ, where $\mathbb{N}$ is the set of natural numbers.
2. Choose the maximum value of R within its range of solutions from the quadratic inequality, that is:

$$R = \lfloor R_{\max} \rfloor \tag{15}$$

   subject to:

$$\frac{N + G_1 + G_2\,(R)}{D\, B} \in \mathbb{N} \tag{16}$$

   where the dependency of G_2 on R comes from (9) and (11). This condition guarantees that the number of symbols after the digital modulator is integer.

If step 2) has no solution, the procedure is repeated by excluding the previous found solutions for N.

3.2.2. Interleaver

When an interleaver is used as ICI mitigation approach, the application of the bound on the number of samples leads to a linear inequality as follows:

$$R\,(N) \leqslant \frac{D\, B}{N + G_1} \tau\, B_w \Rightarrow R\,(N) = \left\lfloor \frac{D\, B}{N + G_1} \tau\, B_w \right\rfloor \tag{17}$$

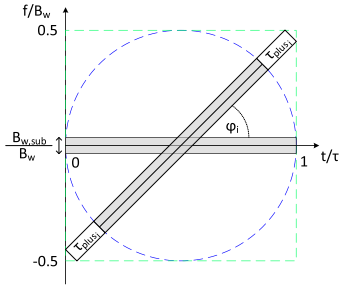

Fig. 6. Waveform optimisation: representation of sub-waveforms with different duration on varying the fractional order.

where, again, the dependency on N is highlighted for clarity. Moreover, by forcing the overlap degree, Q, to be less than a threshold, T, the following constraint on the number of sub-carriers can be obtained:

$$C\,(N) \leqslant \frac{\pi}{2} \frac{1}{\sin^{-1}\left(\dfrac{\beta + 1}{R\,(N)\; T}\right)} \Rightarrow C\,(N) = \left\lfloor \frac{\pi}{2} \frac{1}{\sin^{-1}\left(\dfrac{\beta + 1}{R\,(N)\; T}\right)} \right\rfloor \tag{18}$$

Therefore N can be found by solving the following maximisation problem:

$$\max_N [N \times (C\,(N) - 1)] \quad \text{subject to} \quad \frac{N + G_1}{D\, B} \in \mathbb{N} \tag{19}$$

As before, the condition guarantees that the number of symbols is integer.

3.3. Sub-waveform adaptive duration

As shown in Fig. 3, the FrFT CoRadar pulse does not occupy the entire available bandwidth since it is clearly enclosed in a circle of radius 0.5 in normalised units. In order to maximise the bandwidth occupancy, it is possible to consider sub-waveforms with different time durations depending on the fractional order. This also leads to an increase of the bit rate with no effect on the bit error ratio, at cost of a slightly higher design complexity.

An example of a longer sub-waveform is shown in Fig. 6: it has a rotation angle of $\phi_i = \pi/4$ and a bandwidth $B_{w,sub}$. The fraction of additional time with respect to the duration of the pulse, τ_{plus_i}, is equal to:

$$\tau_{plus_i} = \frac{\tau_i - \tau}{2\tau} \tag{20}$$

where τ_i is the duration of the i-th sub-waveform given by:

$$\tau_i = \begin{cases} \dfrac{\tau}{|\cos(\phi_i)|} & \phi_i \in \left[0, \frac{\pi}{4}\right) \cup \left[\frac{3\pi}{4}, \pi\right) \\ \dfrac{\tau}{|\sin(\phi_i)|} & \phi_i \in \left[\frac{\pi}{4}, \frac{3\pi}{4}\right) \end{cases} \tag{21}$$

$i = 1, \ldots, C - 1$. Thus, the number of bits that the longer i-th sub-waveform can accommodate is given by:

$$N_i = \left\lfloor \frac{D\, B}{R} \tau_i\, B_w \right\rfloor - G \quad \text{s.t.} \quad \frac{N_i + G}{D\, B} \in \mathbb{N} \tag{22}$$

Equation (2) shows a linear relationship between the fractional order α and the rotation angle ϕ. When sub-waveforms with different durations are considered, this equation becomes nonlinear and can be written as:

$$\alpha_i = \frac{2}{\pi} \left[\phi_i + \Gamma\left(\phi_i, \tau_{plus_i}\right)\right] \tag{23}$$

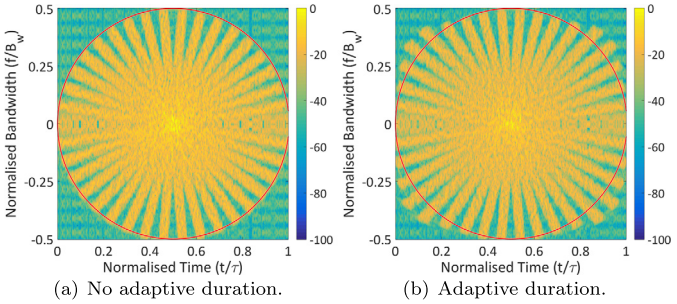

(a) No adaptive duration. (b) Adaptive duration.

Fig. 7. Spectrograms of a FrFT CoRadar waveform (a) without and (b) with adaptive duration.

where

$$\Gamma\left(\phi_i, \tau_{plus_i}\right) = \cos^{-1}\left[\cos\phi_i \left(\frac{\lambda}{1+2\tau_{plus_i}} + \frac{2\tau_{plus_i}}{\lambda\left(1+2\tau_{plus_i}\right)}\right)\right] \tag{24}$$

with

$$\lambda = \sqrt{1+\left(1+2\tau_{plus_i}\right)^2 \tan^2\phi_i} \tag{25}$$

An example of spectrograms of a FrFT CoRadar waveform (a) without and (b) with adaptive duration is shown in Fig. 7. The red circle indicates the time-frequency region occupied by the pulse when no optimisation is applied. In terms of bit rate, the adaptive duration optimisation leads to an improvement of about 10%.

4. Performance evaluation

In this Section the radar and communication performance of the FrFT CoRadar waveform design are evaluated and compared with those obtained with OFDM waveforms, as they are already used in radars and CoRadar systems. Preliminary results are also reported when using reduced PAPR FrFT waveforms, obtained by means of a companding technique. Moreover, a link budget analysis is performed to demonstrate the feasibility of the proposed FrFT based waveform design method for CoRadar system.

4.1. System configuration

This Section describes the configuration of the CoRadar system used for the performance evaluation. For simplicity, a repetition block code is used with $D = 1/L$, where L is the length of the employed Barker codeword.[2] Regarding the interleaver, this is implemented as a matrix filled by rows and emptied by columns [47]. Finally, the pilot waveform is a bi-phase coded signal based on a Coarse/Acquisition (C/A) code [48] given by:

$$p[n] = e^{j\pi\left(a[n]-\frac{1}{4}\right)} \tag{26}$$

where $a[n]$ is the selected C/A code properly up-sampled and truncated to match the length, in samples, of the CoRadar waveform.[3] The OFDM waveforms are generated by using the same framework used for the FrFT waveforms, shown at the top of Fig. 2, in which the FrFT block is replaced by an OFDM block [49]. Note no cyclic prefix was used and the interleaver was removed.

[2] The Barker code is selected for its good autocorrelation properties. However any other sequence with similar properties can be used, and even other correction techniques can be employed.

[3] In case of moving transmitter and/or receiver, carrier offset compensation would also be necessary. Therefore, depending on the application, frequency shifted versions of the pilot waveform may be used.

Table 1
List of the parameters obtained when FrFT optimised and OFDM optimised selection processes are used, respectively.

	FrFT optimised	OFDM optimised
B_w	500 MHz	
τ	9.982 µs	
D	1/7	
B	2 (QPSK)	
G	3	
β	0.4	
$T^\star$	$3/7 = 0.429$	
C	11	16
N	59	
Bit/Pulse	590	885
R	23	
Q	0.428	0.621
$B_{w,sub}$	30.435 MHz	
Δ_f	45.455 MHz	31.250 MHz

Furthermore, two parameters selection processes are considered. The first one, FrFT optimised, is the one previously described in Section 3.2.2 when an interleaver is used. The second one, OFDM optimised, using the same initial parameters, increases the number of sub-carriers, C, in order to optimise the frequency occupancy of the OFDM waveform. Table 1 lists the parameters obtained when the two selection processes are used, respectively. The FrFT optimised parameters selection procedure ensures that $Q \leqslant T$, however the OFDM sub-carrier spacing, Δ_f, is greater than $B_{w,sub}$, which means that frequency gaps are present in the OFDM waveform. On the other hand, the OFDM optimised parameters selection process leads to $\Delta_f \approx B_{w,sub}$, but $Q > T$. Moreover, in both cases the number of bits per sub-carrier, N, is 59, while the number of sub-carriers, C, is 11 and 16, respectively. This means that the bit rate would be $590 \times \mathrm{PRF}$ b/s in the first case, and $885 \times \mathrm{PRF}$ b/s in the second case.

4.2. Radar performance

In order to evaluate the radar performance of the proposed FrFT based CoRadar waveform design, two analyses are carried out. Firstly, parameters such as range resolution, Doppler resolution and Side Lobe Levels (SLLs) are estimated from its Ambiguity Function (AF). Then, by means of a Monte Carlo simulation, the Receiver Operating Characteristic (ROC) for a square law detector is derived. A similar analysis is performed for OFDM waveform and LFM pulse for comparison purposes. In particular, the LFM pulse is designed such that it occupies the same bandwidth, B_w, and has the same duration, τ, of the FrFT and the OFDM CoRadar waveforms.

4.2.1. Ambiguity function

The FrFT's and OFDM's AFs are computed over a Monte Carlo simulation with 100 iterations, since for both of them the actual pulse is affected by the transmitted sequence of random bits. Fig. 8(a) and Fig. 8(b) show the average AFs of the FrFT and the OFDM, respectively, when the FrFT optimised parameters are used. The FrFT's AF has a much flatter shape than the OFDM's, which, instead, presents very high side lobes caused by spectral peaks and valleys between the OFDM sub-carriers. This behaviour is more evident by looking at the zero-Doppler cuts shown in Fig. 8(c) and Fig. 8(d), for the FrFT and the OFDM waveform, respectively, while the zero-delay cuts in Fig. 8(e) and Fig. 8(f) show a similar trend between FrFT, OFDM and LFM waveform, though this changes at different delay cuts. However, lower side lobes are achieved at cost of a slightly worse resolution of the FrFT waveform with respect to OFDM and LFM, both in range and Doppler. Resolutions and side lobe levels are summarised in Table 2, where all the values are taken by assuming a reference level at -3 dB. Moreover, range resolutions are normalised to $0.886 \times \frac{c}{2B_w}$, with c denoting the

Table 2
Radar performance parameters.

	FrFT optimised		OFDM optimised		LFM
	FrFT	**OFDM**	**FrFT**	**OFDM**	
Normalised range res.	1.46	1.01	1.48	1.03	1.01
Normalised Doppler res.	1.30×10^{-4}	0.90×10^{-4}	1.31×10^{-4}	0.90×10^{-4}	0.89×10^{-4}
Zero-Doppler SLL	−16.6 dB	−4.6 dB	−16.5 dB	−9.9 dB	−13.3 dB
Zero-delay SLL	−16.6 dB	−13.3 dB	−16.5 dB	−13.3 dB	−13.3 dB

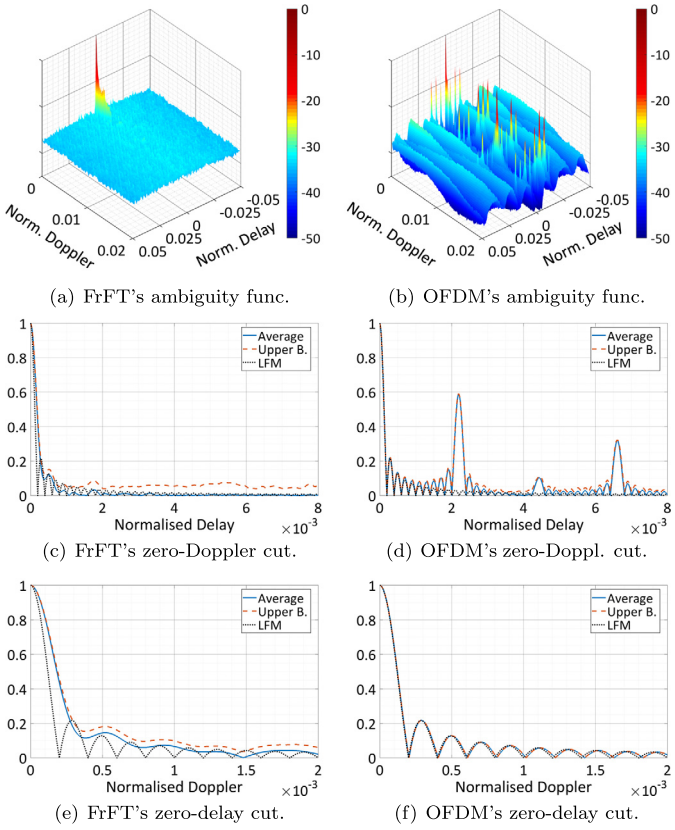

(a) FrFT's ambiguity func. (b) OFDM's ambiguity func. (c) FrFT's zero-Doppler cut. (d) OFDM's zero-Doppl. cut. (e) FrFT's zero-delay cut. (f) OFDM's zero-delay cut.

Fig. 8. Average Ambiguity Functions (AFs) of the (a) FrFT and (b) OFDM waveform when the FrFT optimised parameters are used. Figures (c)–(d) show their zero-Doppler cuts (average, in blue, and upper bound, in red) compared to the LFM's zero-Doppler cut. Figures (e)–(f) show their zero-delay cuts (average, in blue, and upper bound, in red) compared to the LFM's zero-delay cut.

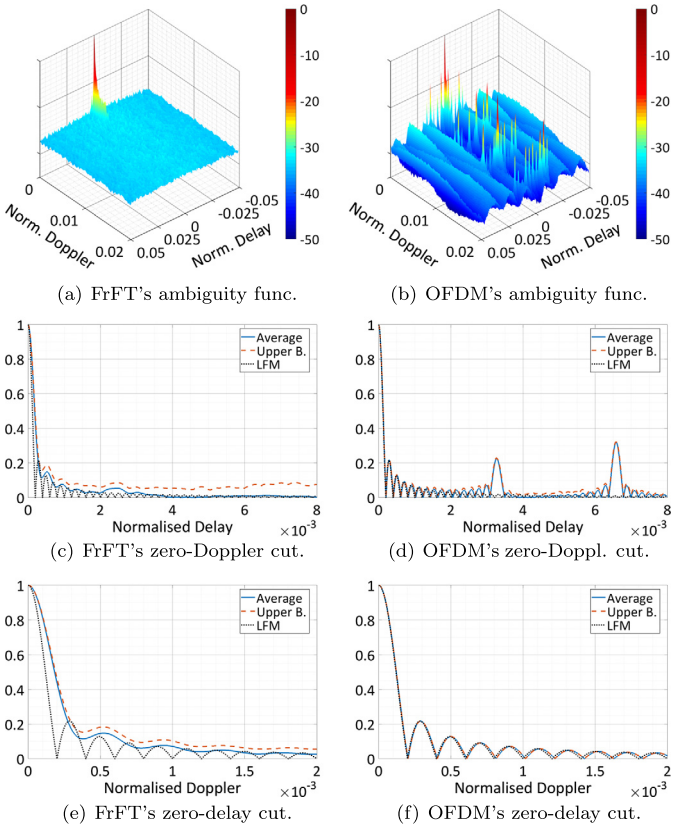

(a) FrFT's ambiguity func. (b) OFDM's ambiguity func. (c) FrFT's zero-Doppler cut. (d) OFDM's zero-Doppl. cut. (e) FrFT's zero-delay cut. (f) OFDM's zero-delay cut.

Fig. 9. Average Ambiguity Functions (AFs) of the (a) FrFT and (b) OFDM waveform when the OFDM optimised parameters are used. Figures (c)–(d) show their zero-Doppler cuts (average, in blue, and upper bound, in red) compared to the LFM's zero-Doppler cut. Figures (e)–(f) show their zero-delay cuts (average, in blue, and upper bound, in red) compared to the LFM's zero-delay cut.

speed of light,[4] while Doppler resolutions are normalised to B_w. Figs. 8(c)–8(f) also report an upper bound for the AF in addition to the average AF, obtained by taking the maximum value for each delay/Doppler bin for all the 100 Monte Carlo iterations. The displacement between the upper bound and the average AF is higher for the FrFT waveform than for the OFDM waveform, showing a higher variability of the former.

The results obtained when the OFDM optimised parameters are used, confirm that the FrFT waveform presents a general better trend in terms of side lobes, but it is outperformed by the OFDM waveform in range and Doppler resolution, as shown in Fig. 9 and reported in Table 2.

4.2.2. Square law detector

The FrFT CoRadar waveform is examined, and compared with OFDM and LFM waveforms, when used for detection purposes with a square law detector. The threshold is selected based on the noise level, namely the Signal-to-Noise Ratio at the Radar receiver, SNR_r, and the desired Probability of False Alarm (P_{FA}). In order to estimate the Receiver Operating Characteristic (ROC) of the detector, a Monte Carlo simulation with 10^5 iterations is carried out. In each iteration, a FrFT based pulse is generated which embeds a random sequence of bits (the same sequence is also used for generating the OFDM based pulse). Since the length of the pulse, in samples, is approximately of 5×10^3 (time-bandwidth product), the total number of Monte Carlo tests is equal to 5×10^8. Fig. 10 compares the performance of the FrFT, OFDM and LFM waveforms when $SNR_r = 20$ dB, and (a) the FrFT optimised and (b) the OFDM optimised parameters are considered. In both cases the FrFT waveform shows performance very close to the LFM. For the OFDM waveform, fixing the Probability of Detection, P_D, to a certain desired level yields a higher P_{FA} compared to the FrFT and LFM waveforms. This is due to the higher range side lobes that its AF presents, as shown in Section 4.2.1.

4.3. Communication performance

Communication performance is expressed in terms of Bit Error Ratio (BER) as a function of energy per bit to noise power spec-

[4] Theoretical range resolution for an ideal chirp evaluated at −3 dB [50].

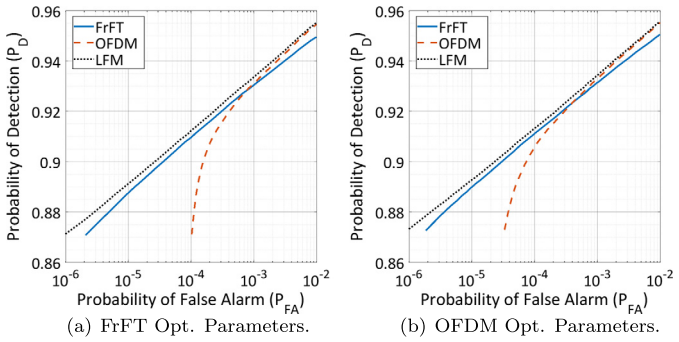

(a) FrFT Opt. Parameters. (b) OFDM Opt. Parameters.

Fig. 10. Receiver Operating Characteristic (ROC) of the square law detector (noise level at $SNR_r = 20$ dB) when FrFT, OFDM and LFM waveforms are used, and when (a) the FrFT optimised and (b) the OFDM optimised parameters are selected.

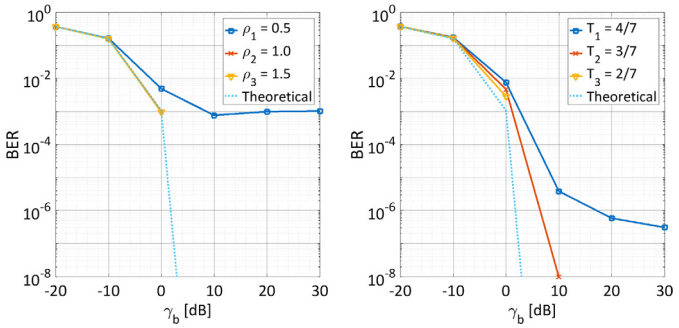

(a) Guard time. (b) Interleaver.

Fig. 11. Performance in terms of BER of the FrFT CoRadar waveform design in presence of AWGN, when (a) a guard time or (b) an interleaver is used as ICI mitigation approach.

tral density ratio [47], i.e. $\gamma_b = SNR_c \times R/(C\,B)$, where SNR_c is the Signal-to-Noise ratio at the Communication receiver. In the following, two analyses are carried out. Firstly, performance for the two different ICI mitigation approaches is evaluated in Additive White Gaussian Noise (AWGN): the objective is to derive conditions for ρ and T that ensure the best performance. The second analysis regards the comparison with the OFDM waveform for different channel models. Note that these analyses do not take into account the relative position between transmitter and receiver, and that both the FrFT and the OFDM pulses are assumed to be already synchronised and their phase compensated.

4.3.1. Guard time and interleaver in AWGN

Communication performance of the FrFT based CoRadar waveform design subject to AWGN when guard time and interleaver are used as ICI mitigation approach, respectively, is evaluated and shown in Fig. 11. The curves are obtained by means of a Monte Carlo simulation during which 10^8 bits are sent. The parameters selection process described in Section 3.2 is used with different values of ρ and T, for guard time and interleaver, respectively. The resulting parameters are summarised in Table 3.

The lower bound, represented by the light blue dotted line, is the BER obtained when the chirp sub-carriers are considered independent, and no ICI is present, and the noise that affects each of them is still AWGN. This is equivalent to the BER of a QPSK modulation (employed in these simulations) taking into account that the coding technique used can correct up to $\lfloor L/2 \rfloor$ errors per codeword. When guard time is used as ICI mitigation approach, as expected the BER decreases as the parameters ρ increases. In fact, $\rho < 1$ means that part of the region affected by ICI is still used to send information bits, thus more errors are expected. In particular a BER floor is visible for $\rho_1 = 0.5$. This is due to errors that are independent of the noise level and are only caused by ICI. Conversely, when $\rho > 1$ the guard time is larger than the region affected by ICI, hence the sub-carriers can be considered independent and the BER approaches the lower bound.[5] Similar results are obtained when the interleaver is used as ICI mitigation method, where the BER decreases as T decreases, since there is less overlap of the chirp sub-carriers. Interesting is that for $T \leqslant T^\star = 3/7$, the BER does not present a plateau anymore (which is visible for $T_1 = 4/7$) and approaches the lower bound. This happens because with $T \leqslant 3/7$ the number of expected errors per codeword is less or equal than which the coding technique can correct, therefore the sub-carriers can be considered independent.

Table 3
List of the parameters for the two ICI mitigation approaches, Guard Time and Interleaver, respectively, and on varying ρ and T.

			Parameters			
			N	C	Bit/pulse	R
G. time	ρ	0.5	54	14	756	12
		1.0	30	12	360	22
		1.5	21	11	231	32
Interl.	T	4/7	53	16	848	25
		3/7	59	11	649	23
		2/7	27	15	405	47

4.3.2. Comparison with OFDM

In this Section the communication performance of the FrFT CoRadar waveform is compared with the performance obtained with the OFDM waveform. The signal is assumed to experience a slow-flat fading, therefore a time-invariant narrowband channel model is considered. Let $\mathbf{s_{tx}}$ be the vector which contains the transmitted signal samples, i.e. $\mathbf{s_{tx}} = [s_{tx}[1], \ldots, s_{tx}[U]]$. The received signal can be written as:

$$\mathbf{s_{rx}} = \mathbf{h} \circ \mathbf{s_{tx}} + \boldsymbol{\zeta} \tag{27}$$

where $\mathbf{h}$ is the vector that contains the channel coefficients, $\boldsymbol{\zeta}$ is the white Gaussian noise and the operator $\circ$ indicates the Hadamard, or entrywise, product. The complex elements of the vector $\mathbf{h}$ are drawn from a statistical distribution whose parameters depend on the propagation path. In addition to the AWGN only scenario for which $h = 1$, three other cases are considered. In case of existence of the Line of Sight (LOS) path, the channel is modelled as Rician with a Rice factor of 4 dB. Conversely, when no LOS path exists, the channel coefficients $\mathbf{h}$ are drawn from a Rayleigh distribution with scale parameter $\sqrt{2}/2$. Finally, in order to take into account shadowing and diffraction that can occur in bad weather conditions, a combination of Rice and Lognormal is considered [51]. In this case the channel coefficients are obtained as the product of a Rice process normalised in power and a Lognormal variable, whose associated Gaussian variable has a standard deviation of 4 (dB spread).

Assuming that the received signal has been equalised, the communication performance is evaluated in terms of BER vs γ_b [dB] in Fig. 12. As before, a Monte Carlo simulation is run during which 10^7 bits are sent. The blue lines refer to the FrFT waveform, while the red lines to the OFDM. Solid lines and dotted lines refer to the cases in which FrFT optimised and OFDM optimised parameters are used, respectively. In the presence of AWGN only, as shown in Fig. 12(a), the FrFT waveform is outperformed by the OFDM. Moreover, a plateau can be observed for the FrFT waveform when OFDM optimised parameters are used, which confirms the results

[5] Note that, here and in the following, some curves are incomplete due to the limited number of bits generated during the simulations.

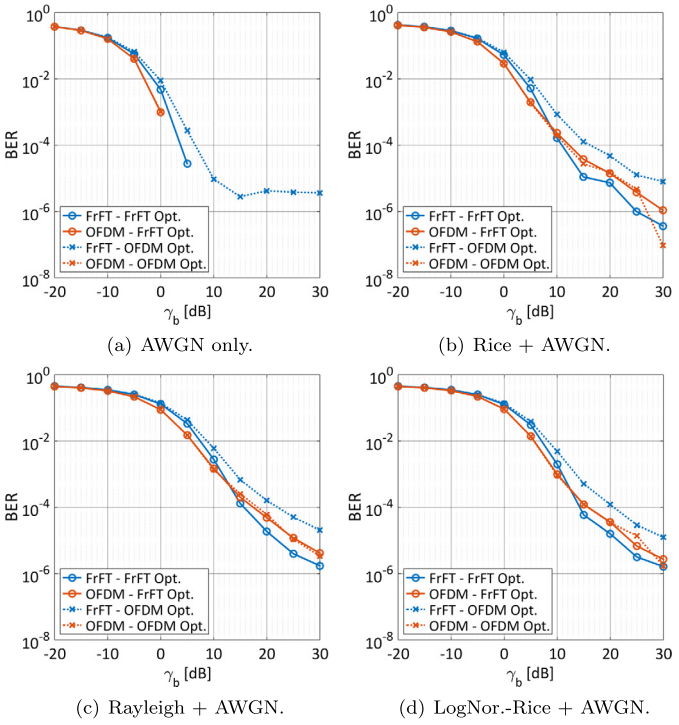

Fig. 12. Communication performance. Comparison between FrFT waveform and OFDM waveform on varying the parameters selection process and for four different channel models: (a) AWGN only, (b) Rice channel, (c) Rayleigh channel and (d) LogNormal-Rice channel.

obtained in Section 4.3.1 since $Q > T^\star$. For all the analysed channel models, the OFDM is not affected by the selected parameters, while the FrFT, as expected, shows better performance when FrFT optimised parameters are used, as they ensure that the overlap is lower than $T^\star = 0.429$. However, even when OFDM optimised parameters are used, for which $Q = 0.621 > T^\star$ but more information bits are sent (see Table 1), the FrFT's BER is still comparable with the OFDM's.

The objective of the analysis above was mainly to show the comparable performance between FrFT and OFDM waveforms with a similar setup. However, it is worth mentioning that replacing the repetition block code with a stronger one, as also mentioned in Section 4.1, or employing a different digital modulation rather than QPSK, could lead to improved BER and/or data rate.

4.4. Reduced peak-to-average power ratio

One drawback of applying the proposed multiplexing scheme is the high PAPR governing the envelope of the transmitted signal, which is due to the fact that most of the energy is concentrated at the centre of the signal, namely in the overlapping area. This phenomenon can lead to non-linear distortions due to the use of High-Power Amplifiers (HPAs), which shall be driven as close to their saturation point as possible in order to operate in maximum efficiency [52]. A possible way to reduce the PAPR of the proposed waveform is by companding the signal in transmission, and de-companding it before demodulation at the communication receiver. In this Section a preliminary analysis is conducted to assess the radar and communication performance of the FrFT waveform when a non-linear companding function is applied. Specifically, an exponential companding is used [53], such that the transmitted waveform, $\tilde{\mathbf{s}}_{\mathbf{tx}}$, can be written as:

$$\tilde{\mathbf{s}}_{\mathbf{tx}} = \sqrt[d]{|\mathbf{s}_{\mathbf{tx}}|} e^{j\theta} \tag{28}$$

Table 4
PAPR for companded FrFT waveforms.

	Average	Min	Max
$d = 1$	12.24 dB	9.91 dB	16.60 dB
$d = 2$	6.89 dB	5.70 dB	9.15 dB
$d = 3$	4.79 dB	3.94 dB	6.24 dB

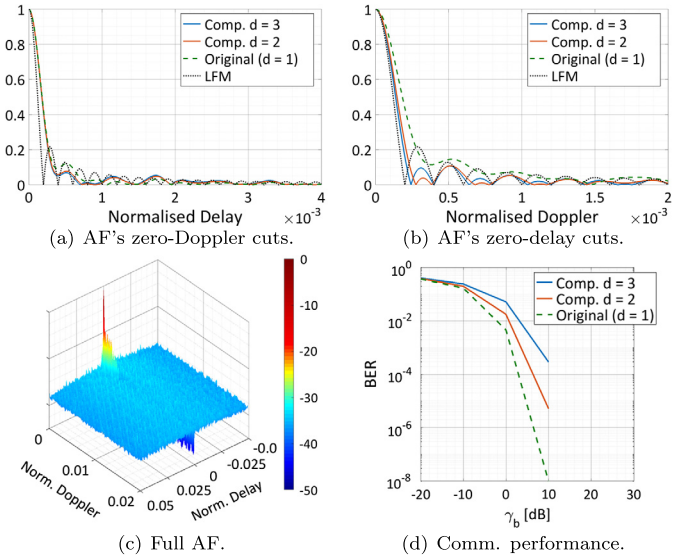

Fig. 13. PAPR reduction. Comparison between the unmodified FrFT waveform ($d = 1$) and the companded pulses with $d = 2$ and $d = 3$, in terms of AF's (a) zero-Doppler and (b) zero-delay cuts, and (c) communication performance in AWGN. For completeness, (d) the full average AF of the companded FrFT pulse with $d = 3$ is reported.

where $\theta = \angle \mathbf{s}_{\mathbf{tx}}$ is the phase of the signal before companding. A comparison is made between the unmodified FrFT waveform, namely with $d = 1$, and the companded FrFT pulses with $d = 2$ and $d = 3$. The average PAPR of the original waveform, computed on 10^6 instances, is equal to 12.24 dB, and it reduces to 6.89 dB and 4.79 dB for $d = 2$ and $d = 3$, respectively; maximum and minimum PAPR are also reported in Table 4. Fig. 13(a) and Fig. 13(b) compare the AF's zero-Doppler and zero-delay cuts of the three waveforms, while Fig. 13(d) shows the communication performance in AWGN when FrFT optimised parameters are used. For completeness, Fig. 13(c) depicts the full AF of the companded pulse when $d = 3$. Both the AF's cuts show small improvements in terms of side lobe levels, as well as an enhanced Doppler resolution, at cost of a slight degradation of the BER. On the other hand, the use of PAPR reduced FrFT waveforms would probably allow the HPA to operate in compression/saturation, gaining in terms of transmitted power, therefore achieving comparable communication performance with respect to the unmodified FrFT waveforms, since simulations provided no errors for γ_b above 10 dB.

4.5. Link budget

In order to validate the feasibility of the proposed FrFT based waveform design for CoRadar system, a link budget analysis is carried out. Signal-to-Noise Ratio at the Radar receiver, SNR_r, and energy per bit to noise power spectral density, γ_b, are chosen depending on the desired radar and communication performance, as shown in Section 4.2 and Section 4.3. For example, according to Fig. 10(a), an $SNR_r = 20$ dB can ensure a probability of false alarm of 5×10^{-6} and a probability of detection of 0.88. Then, assuming that a PRF = 3 kHz is used, an average power of $P_t = 50$ W is sent, and using the FrFT optimised parameters as in Table 1, the max-

Table 5
Link Budget Parameters.

Param.	Description	Value
PRF	Pulse Repetition Frequency.	3 kHz
P_t	Transmitted average power.	50 W
λ_r	Wavelength.	3 cm
k	Boltzmann's constant.	$1.38 \cdot 10^{-23}$ J/K
T_0	Noise reference temperature.	290 K
SNR_r	SNR at radar receiver.	20 dB
$G_{t,main}$	Radar transmitting antenna's gain in the main lobe.	35 dB
$G_{r,radar}$	Radar receiving antenna's gain.	35 dB
σ	Radar cross section.	1 m^2
L_s	Loss factor.	0.4
n	Number of pulses incoherently combined.	64
G_{sp}	Signal processing gain.	37 dB
F_{radar}	Radar's noise figure.	4 dB
r_{max}	Maximum radar range.	22.14 km
γ_b	Energy per bit to noise power spectral density.	20 dB
SNR_c	SNR at communication receiver.	19.81 dB
$G_{t,side}$	Radar transmitting antenna's gain in the side lobe.	5 dB
$G_{r,comms}$	Communication receiving antenna's gain.	15 dB
F_{comms}	Communication receiver's noise figure.	10 dB
d_{max}	Maximum radar–communication receiver distance.	22.26 km

imum radar range, r_{max}, and the maximum radar–communication receiver distance, d_{max}, are obtained. For this specific analysis, the radar link budget is obtained by rearranging the radar range equation as follows:

$$r_{max} = \left(\frac{P_t}{\tau PRF} \frac{\lambda_r^2 \sigma L_s}{(4\pi)^3 k T_0 B_w SNR_r} \frac{G_{t,main} G_{r,radar}}{F_{radar}} n^{0.5} G_{sp} \right)^{1/4} \tag{29}$$

while the communication link budget is:

$$d_{max} = \left(\frac{P_t}{\tau PRF} \frac{G_{t,side} G_{r,comms} \lambda_r^2}{F_{comms} (4\pi)^2 k T_0 B_w SNR_c} \right)^{1/2} \tag{30}$$

All the parameters are listed in Table 5. It is worth noting that the communication link budget is evaluated assuming that the communication receiver is placed in the side lobe of the radar's antenna beam. With this configuration, a target with a radar cross section of 1 m^2 can be detected at a maximum range of $r_{max} = 22.14$ km with a probability of detection of about 0.88. At the same time, a data stream of 1.947 Mb/s can be directed to a communication receiver placed in the radar antenna's side lobe at a distance of $d_{max} = 22.26$ km, ensuring a BER lower than 10^{-4}. Longer radar range and radar–communication receiver distance may be obtained, for example, by decreasing the bandwidth of the signal B_w, therefore trading them off for the range resolution and the data rate, respectively.

5. Hardware implementation

An implementation of the proposed FrFT CoRadar system on a Software Defined Radio (SDR) device has been presented in [54]. The prototype consists of a mono-static radar that generates the FrFT waveforms, sends the pulses and performs basic radar tasks, and a separate communication receiver that demodulates the pulses. The prototype is highly flexible, since all the parameters described in this paper can be set, and demonstrates the feasibility of the proposed waveform design. However, it suffers from the computation complexity of the discrete FrFT, limiting the PRF and allowing to generate only waveforms with few sub-carriers.

The FrFT CoRadar prototype has been used in a controlled laboratory environment to acquire data and assess its radar and communication capabilities. The ICI mitigation approach based on the

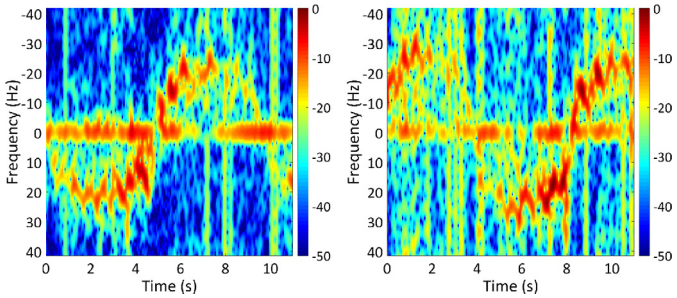

(a) $C = 4$, $SNR_r = 14\,dB$. (b) $C = 8$, $SNR_r = 14\,dB$.

Fig. 14. Snapshots of the real-time spectrogram computed from FrFT Co-Radar pulses. (a) $C = 4$ sub-carriers, person walking towards the radar approximately between 0–5 seconds and 10–11 s, and away from it between 5–10 s. (b) $C = 8$ sub-carriers, person walking towards the radar approximately between 4–8 s, and away from it between 0–4 s and 8–11 s.

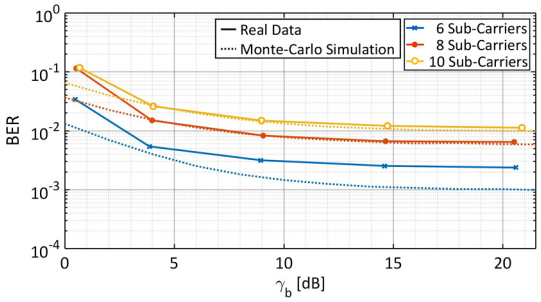

Fig. 15. Communication performance evaluated on real data, on varying γ_b and for different number of sub-carriers.

interleaver has been used and the parameters have been set as follows: wavelength $\lambda_r = 10$ cm, bandwidth $B_w = 1$ MHz, pulse duration $\tau = 378$ µs, $N = 3$ information bits and $G = 3$ guard bits per sub-carrier, $L = 7$ the length of the Barker code, QPSK is the selected modulation scheme, $\beta = 0.4$ and $R = 18$ are the roll-off and the up-sampling factors of the RRC filter, respectively, and PRF = 83.33 Hz. Due to the limited power and bandwidth resources of the employed SDR device, the radar capability of the system is assessed by computing a real-time spectrogram from the received pulses. During the acquisitions a human target was walking towards and away from the radar, and its Doppler and micro-Doppler signature can be clearly seen from the snapshots of the real-time spectrogram in Fig. 14(a) and Fig. 14(b), for $C = 4$ and $C = 8$ sub-carriers, respectively. Communication performance is also evaluated in terms of BER on varying the estimated energy per bit to noise power spectral density, γ_b, and compared with results obtained with a Monte Carlo simulation assuming a Rice channel with K-factor equal to 6 dB (indoor channel) in Fig. 15. Results on real and simulated data are consistent, with BER that decreases as γ_b increases and the number of sub-carriers, C, decreases.

6. Practical challenges

Despite demonstrating the feasibility of the proposed FrFT based CoRadar framework in Section 5, some practical challenges still have to be addressed in order to obtain a full working system. In this Section a non-comprehensive list of them is presented.

The first one concerns the computation of the discrete FrFT. This topic has been widely investigated in the literature [55,56] but, even if algorithms with complexity $O(U \log U)$ (with U length of the signal) have been proposed [57], they approximate the continuous FrFT rather than representing fast algorithms for the computation of the discrete FrFT (as the Fast Fourier Transform (FFT) algorithm is for the ordinary discrete Fourier transform). A method

for the discrete FrFT computation with complexity $O\left(U^2\right)$ is presented in [58], and it has been used in [54] for prototype development. However, as mentioned earlier, due to its high computational cost this implementation of the discrete FrFT limits the generation of waveforms with either a high number of sub-carriers or a high time-bandwidth product. For this reason, either a new formulation of discrete FrFT is sought or an ad-hoc and clever hardware implementation of an existing algorithm is required.

Clutter cancellation and mitigation of the Range Side lobe Modulation (RSM) effect that occurs because of the transmission of different pulses each PRI, are two other practical challenges. Common matched filter processing at the radar receiver would produce range side lobes that are different for each waveform, leading to the problem of clutter dispersion for which standard clutter cancellation techniques are ineffective. Different approaches have been proposed for pulse agility radars and may be adapted to the proposed FrFT CoRadar system. In [59] the RSM effect is mitigated by mismatch filtering the different waveforms sent in a Coherent Processing Interval (CPI) in order to obtain similar range side lobe responses. In particular an iterative procedure for the joint design of multiple receiver filters is presented. This technique is also recalled in [60], where the authors propose a closed-form rather than iterative solution specifically adapted for Moving Target Indication (MTI) radars. A more general framework for dealing with the problem of RSM is proposed in [61], whose aim is the optimisation of the Cross Ambiguity Function (CAF) at cost, however, of a higher computational complexity.

Other problems concern the deep fade that the communication receiver may experience as it moves through the radiation beam pattern of the radar's antenna, and the reduction of the PAPR. With this regards, preliminary results have been reported in Section 4.4 by using an exponential companding technique, however other solutions can be examined and evaluated.

7. Conclusions

A novel concept of joint radar–communication (CoRadar) system based on the Fractional Fourier Transform (FrFT) was presented. The proposed waveform design technique directly embeds data into the radar waveform, allowing the two operations, radar and communication, to run simultaneously. The method exploits the FrFT to map modulated signal, i.e. QPSK signals, into chirp sub-carriers with different chirp rates. This also makes the system fully scalable, since its configuration can be adapted to the available bandwidth, pulse length and condition of the channel. In particular, procedures for parameters selection driven by the radar requirements were explained, along with two waveform optimisation techniques aiming at minimising the effect of the Inter-Carrier Interference (ICI) and maximising the data rate.

Radar and communication performance of the proposed waveform design were assessed and compared with an OFDM CoRadar system, that presents a comparable bit rate. Results showed that the FrFT waveform presents performance closer to a Linear Frequency Modulated (LFM) pulse than OFDM waveform in terms of probability of detection and probability of false alarm, slightly trading range and Doppler resolutions. Communication performance confirmed the viability of the proposed waveform design, showing comparable Bit Error Ratios (BERs) with the OFDM waveform in all the analysed cases. A link budget analysis was also conducted to prove the feasibility of the FrFT based waveform design for CoRadar system. Finally, a prototype of the proposed FrFT CoRadar system was presented, and radar and communication performance were evaluated by means of data acquired in a real controlled laboratory environment.

The FrFT CoRadar technology is suitable for a wide range of applications, but it needs to be further investigated. A stress analysis in presence of clutter is necessary in order to definitely validate the concept, and an investigation of possible clutter cancellation techniques needs to be carried out. Furthermore, practical problems must be addressed, such as the fast computation of the discrete FrFT and the mitigation of the Range Side lobe Modulation (RSM) effect.

Acknowledgments

This work was supported by the Engineering and Physical Sciences Research Council (EPSRC) Grant number EP/K014307/1 and the MOD University Defence Research Collaboration in Signal Processing.

References

[1] C. Sturm, W. Wiesbeck, Waveform design and signal processing aspects for fusion of wireless communications and radar sensing, Proc. IEEE 99 (7) (2011) 1236–1259.
[2] S. Quan, W. Qian, J. Guq, V. Zhang, Radar-communication integration: an overview, in: 2014 IEEE 7th International Conference on Advanced Infocomm Technology (ICAIT), Fuzhou, China, 2014, pp. 98–103.
[3] M. Fossi, M. Gherardelli, OFDM radar signals for both surveillance and navigation aids to landing aircrafts, in: 2012 Tyrrhenian Workshop on Advances in Radar and Remote Sensing (TyWRRS), Naples, Italy, 2012, pp. 46–52.
[4] A. Aubry, A.D. Maio, Y. Huang, M. Piezzo, A. Farina, A new radar waveform design algorithm with improved feasibility for spectral coexistence, IEEE Trans. Aerosp. Electron. Syst. 51 (2) (2015) 1029–1038.
[5] A. Aubry, A.D. Maio, M.M. Naghsh, Optimizing radar waveform and Doppler filter bank via generalized fractional programming, IEEE J. Sel. Top. Signal Process. 9 (8) (2015) 1387–1399.
[6] K.-W. Huang, M. Bică, U. Mitra, V. Koivunen, Radar waveform design in spectrum sharing environment: coexistence and cognition, in: 2015 IEEE International Radar Conference (RadarCon), Arlington, VA, USA, 2015, pp. 1698–1703.
[7] H.T. Hayvaci, B. Tavli, Spectrum sharing in radar and wireless communication systems: a review, in: 2014 International Conference on Electromagnetics in Advanced Applications (ICEAA), Palm Beach, FL, USA, 2014, pp. 810–813.
[8] S. Kim, J.M.J. Park, K. Bian, PSUN: an OFDM scheme for coexistence with pulsed radar, in: 2015 International Conference on Computing, Networking and Communications (ICNC), Anaheim, CA, USA, 2015, pp. 984–988.
[9] H. Griffiths, L. Cohen, S. Watts, E. Mokole, C. Baker, M. Wicks, S. Blunt, Radar spectrum engineering and management: technical and regulatory issues, Proc. IEEE 103 (1) (2015) 85–102.
[10] R. Cager, D. LaFlame, L. Parode, Orbiter Ku-band integrated radar and communications subsystem, IEEE Trans. Commun. 26 (11) (1978) 1604–1619.
[11] W. Wiesbeck, L. Sit, M. Younis, T. Rommel, G. Krieger, A. Moreira, Radar 2020: the future of radar systems, in: 2015 IEEE International Geoscience and Remote Sensing Symposium (IGARSS), Milan, Italy, Springer, 2015, pp. 188–191.
[12] J. Proakis, Digital Communications, Electrical Engineering Series, McGraw-Hill, 2001.
[13] A. Turlapaty, Y. Jin, A joint design of transmit waveforms for radar and communications systems in coexistence, in: 2014 IEEE Radar Conference (RadarCon), Cincinnati, OH, USA, 2014, pp. 315–319.
[14] S.C. Surender, R.M. Narayanan, UWB noise-OFDM netted radar: physical layer design and analysis, IEEE Trans. Aerosp. Electron. Syst. 47 (2) (2011) 1380–1400.
[15] L. Han, K. Wu, Joint wireless communication and radar sensing systems – state of the art and future prospects, IET Microw. Antennas Propag. 7 (11) (2013) 876–885.
[16] B. Cantrell, J. Coleman, G. Trunk, Radar Communications, Tech. rep., DTIC Document, 1981.
[17] M. Skolnik, G. Linde, K. Meads, Senrad: an advanced wideband air-surveillance radar, IEEE Trans. Aerosp. Electron. Syst. 37 (4) (2001) 1163–1175.
[18] J. Moghaddasi, K. Wu, Multifunctional transceiver for future radar sensing and radio communicating data-fusion platform, IEEE Access 4 (2016) 818–838.
[19] S.J. Xu, Y. Chen, P. Zhang, Integrated radar and communication based on DS-UWB, in: 2006 3rd International Conference on Ultrawideband and Ultrashort Impulse Signals, Sevastopol, Ukraine, 2006, pp. 142–144.
[20] M. Roberton, E.R. Brown, Integrated radar and communications based on chirped spread-spectrum techniques, in: 2003 IEEE MTT-S International Microwave Symposium Digest, vol. 1, Philadelphia, PA, USA, 2003, pp. 611–614.
[21] G.N. Saddik, R.S. Singh, E.R. Brown, Ultra-wideband multifunctional communications/radar system, IEEE Trans. Microw. Theory Tech. 55 (7) (2007) 1431–1437.
[22] F. Hu, G. Cui, W. Ye, L. Kong, Y. Huang, L. Yuan, Integrated radar and communication system based on stepped frequency continuous waveform, in: 2015 IEEE International Radar Conference (RadarCon), Arlington, VA, USA, 2015, pp. 1084–1087.

[23] Z. Zhao, D. Jiang, A novel integrated radar and communication waveform based on LFM signal, in: 2015 5th International Conference on Electronics Information and Emergency Communication (ICEIEC), Beijing, China, 2015, pp. 219–223.
[24] N. Levanon, E. Mozeson, Radar Signals, John Wiley & Sons, 2004.
[25] B.J. Donnet, I.D. Longstaff, Combining MIMO radar with OFDM communications, in: 2006 European Radar Conference (EuRAD), Manchester, UK, 2006, pp. 37–40.
[26] C. Sturm, T. Zwick, W. Wiesbeck, An OFDM system concept for joint radar and communications operations, in: 2009 69th Vehicular Technology Conference (VTC), Barcelona, Spain, 2009, pp. 1–5.
[27] T. Jiang, Y. Wu, An overview: peak-to-average power ratio reduction techniques for OFDM signals, IEEE Trans. Broadcast. 54 (2) (2008) 257–268.
[28] B.S. Krongold, D.L. Jones, PAR reduction in OFDM via active constellation extension, IEEE Trans. Broadcast. 49 (3) (2003) 258–268.
[29] J. Euzière, R. Guinvarc'h, M. Lesturgie, B. Uguen, R. Gillard, Dual function radar communication time-modulated array, in: 2014 International Radar Conference (Radar), Lille, France, 2014, pp. 1–4.
[30] A. Hassanien, M.G. Amin, Y.D. Zhang, F. Ahmad, Dual-function radar–communications: information embedding using sidelobe control and waveform diversity, IEEE Trans. Signal Process. 64 (8) (2016) 2168–2181.
[31] A. Hassanien, M.G. Amin, Y.D. Zhang, F. Ahmad, Dual-function radar–communications using phase-rotational invariance, in: 2015 23rd European Signal Processing Conference (EUSIPCO), Nice, France, 2015, pp. 1346–1350.
[32] D. Gaglione, C. Clemente, C.V. Ilioudis, A.R. Persico, I.K. Proudler, J.J. Soraghan, Fractional Fourier based waveform for a joint radar–communication system, in: 2016IEEE Radar Conference (RadarCon), Philadelphia, PA, USA, 2016, pp. 1–6.
[33] C. Clemente, I. Shorokhov, I. Proudler, J.J. Soraghan, Radar waveform libraries using fractional Fourier transform, in: 2014 IEEE Radar Conference (RadarCon), Cincinnati, OH, USA, 2014, pp. 855–858.
[34] C. Clemente, C. Ilioudis, D. Gaglione, K. Thompson, S. Weiss, I. Proudler, J.J. Soraghan, Reuse of fractional waveform libraries for MIMO radar and electronic countermeasures, in: 2014 6th International Symposium on Communications, Control and Signal Processing (ISCCSP), Athens, Greece, 2014, pp. 505–508.
[35] C.V. Ilioudis, C. Clemente, I. Proudler, J.J. Soraghan, Constant envelope fractional fourier transform based waveform libraries for MIMO radar, in: 2014 Sensor Signal Processing for Defence (SSPD), Edinburgh, UK, 2014, pp. 1–5.
[36] C.V. Ilioudis, C. Clemente, I. Proudler, J.J. Soraghan, Performance analysis of fractional waveform libraries in MIMO radar scenario, in: 2015 IEEE International Radar Conference (RadarCon), Arlington, VA, USA, 2015, pp. 1119–1124.
[37] X. Zhang, K. Wang, Y. Gao, X. Liu, Optimal waveform design oriented toward cognitive radar in fractional Fourier domain, in: 2016 IEEE Radar Conference (RadarCon), Philadelphia, PA, USA, 2016, pp. 1–5.
[38] X. Chen, J. Guan, Z. Bao, Y. He, Detection and extraction of target with micromotion in spiky sea clutter via short-time fractional Fourier transform, IEEE Trans. Geosci. Remote Sens. 52 (2) (2014) 1002–1018.
[39] C. Clemente, J.J. Soraghan, Range Doppler and chirp scaling processing of synthetic aperture radar data using the fractional Fourier transform, IET Signal Process. 6 (5) (2012) 503–510.
[40] G.A.B. Khadher, A.C. Zidouri, OFDM synthetic aperture radar based on fractional Fourier transform, in: 2016 13th International Multi-Conference on Systems, Signals Devices (SSD), Leipzig, Germany, 2016, pp. 165–170.
[41] M. Martone, A multicarrier system based on the fractional Fourier transform for time-frequency-selective channels, IEEE Trans. Commun. 49 (6) (2001) 1011–1020.
[42] Y. Chen, C. Clemente, J.J. Soraghan, S. Weiss, Partial fractional Fourier transform (PFRFT)-OFDM for underwater acoustic communication, in: 2015 23rd European Signal Processing Conference (EUSIPCO), Nice, France, 2015, pp. 364–368.
[43] V. Namias, The fractional order Fourier transform and its application to quantum mechanics, IMA J. Appl. Math. 25 (3) (1980) 241–265.
[44] H.M. Ozaktas, Z. Zalevsky, M.A. Kutay, The Fractional Fourier Transform with Applications in Optics and Signal Processing, Wiley, Chichester, 2001.
[45] L.B. Almeida, The fractional Fourier transform and time-frequency representations, IEEE Trans. Signal Process. 42 (11) (1994) 3084–3091.
[46] D. Manolakis, V. Ingle, Applied Digital Signal Processing: Theory and Practice, Cambridge University Press, 2011.
[47] A. Goldsmith, Wireless Communications, Cambridge University Press, 2005.
[48] GPS ICD, Global Positioning Systems Directorate System Engineering & Integration Interface Specification IS-GPS-200H, Navstar GPS Space Segment/Navigation User Interfaces.
[49] M. Rice, Digital Communications: A Discrete-Time Approach, Pearson/Prentice Hall, 2009.
[50] I.G. Cumming, F.H. Wong, Digital Processing of Synthetic Aperture Radar Data: Algorithms and Implementation, Artech House Remote Sensing Library, Artech House, Boston, 2005.
[51] G. Corazza, C. Ferrarelli, F. Vatalaro, A rice-lognormal terrestrial and satellite channel model, in: 1994 Third Annual International Conference on Universal Personal Communications, San Diego, CA, USA, 1994, pp. 155–159.
[52] E. Costa, M. Midrio, S. Pupolin, Impact of amplifier nonlinearities on OFDM transmission system performance, IEEE Commun. Lett. 3 (2) (1999) 37–39.
[53] T. Jiang, Y. Yang, Y.-H. Song, Exponential companding technique for PAPR reduction in OFDM systems, IEEE Trans. Broadcast. 51 (2) (2005) 244–248.
[54] D. Gaglione, C. Clemente, A.R. Persico, C.V. Ilioudis, I. Proudler, J.J. Soraghan, Fractional Fourier transform based co-radar waveform: experimental validation, in: 2016 Sensor Signal Processing for Defence (SSPD), Edinburgh, UK, 2016, pp. 1–5.
[55] X. Yang, Q. Tan, X. Wei, Y. Xiang, Y. Yan, G. Jin, Improved fast fractional-Fourier-transform algorithm, J. Opt. Soc. Am. A 21 (9) (2004) 1677–1681.
[56] A. Koc, H.M. Ozaktas, C. Candan, M.A. Kutay, Digital computation of linear canonical transforms, IEEE Trans. Signal Process. 56 (6) (2008) 2383–2394.
[57] A. Bultheel, H.E.M. Sulbaran, Computation of the fractional Fourier transform, Appl. Comput. Harmon. Anal. 16 (3) (2004) 182–202.
[58] C. Candan, M.A. Kutay, H.M. Ozaktas, The discrete fractional Fourier transform, IEEE Trans. Signal Process. 48 (5) (2000) 1329–1337.
[59] S.D. Blunt, M.R. Cook, J. Stiles, Embedding information into radar emissions via waveform implementation, in: 2010 International Waveform Diversity and Design Conference, Niagara Falls, ON, Canada, 2010, pp. 195–199.
[60] A.C. O'Connor, J.M. Kantor, J. Jakabosky, Joint equalization filters that mitigate waveform-diversity modulation of clutter, in: 2016 IEEE Radar Conference (RadarCon), Philadelphia, PA, USA, 2016, pp. 1–6.
[61] D.P. Scholnik, Range-ambiguous clutter suppression with pulse-diverse waveforms, in: 2011 IEEE Radar Conference (RadarCon), Kansas City, MO, USA, 2011, pp. 336–341.

Domenico Gaglione received the B.Sc. (*cum laude*) and M.Sc. (*cum laude*) degrees from Università degli Studi di Napoli "Federico II", Naples, Italy, in 2011 and 2013, respectively, in Telecommunications Engineering. In 2017 he obtained the Ph.D. degree from the Department of Electronic and Electrical Engineering, University of Strathclyde, Glasgow, UK, where he also worked as Research Assistant since 2016. He is currently a Junior Scientist at the NATO STO Centre for Maritime Research & Experimentation (CMRE), La Spezia, Italy. His research interests include joint radar–communication systems, micro-Doppler based and SAR based classification and identification, radar waveform design, and statistical signal processing with emphasis on target tracking and data fusion.

Dr. Gaglione received the First Prize at the Student Paper Competition of the 2015 IEEE International Radar Conference, Arlington, VA, USA.

Carmine Clemente received the Laurea cum laude (B.Sc.) and Laurea Specialistica cum laude (M.Sc.) degrees in telecommunications engineering from Università degli Studi del Sannio, Benevento, Italy, in 2006 and 2009, respectively. He received the Ph.D. degree from the Department of Electronic and Electrical Engineering, University of Strathclyde, Glasgow, UK, in 2012.

Currently, he is a Lecturer in the Department of Electronic and Electrical Engineering, University of Strathclyde, Glasgow, UK working on advanced Radar signal processing algorithm, MIMO radar systems, and micro-Doppler analysis. His research interests include synthetic aperture radar focusing and bistatic SAR focusing algorithms development, micro-Doppler signature analysis and extraction from multistatic radar platforms, micro-Doppler classification, and statistical signal processing.

Christos V. Ilioudis was born in Thessaloniki, Greece, on August 25, 1988. He received the Diploma degree from the Department of Informatics and Telecommunications Engineering, University Of Western Macedonia, Kozani, Greece, in 2012 and the M.Sc. degree with distinction in electronics and electrical engineering from the University of Strathclyde, Glasgow, UK, in 2013. He received his Ph.D. degree at the Centre in Signal and Image Processing, Department of Electronic and Electrical Engineering, University of Strathclyde, 2017. Currently he is a Research Associate on the UDRC phase II work package 4 within LSSC consortium, with research focused on the design of novel waveform libraries and paradigms specialised for Distributed MIMO Radar Systems. His current research interests include MIMO radar systems, ambiguity function shaping, joint radar communication systems, and orthogonal chirp division multiplexing.

Mr. Ilioudis received the third position in the best student paper competition at IEEE International Radar Conference 2015, Arlington, USA. Also, his paper was within the ten best papers (finalists) in the same competition at IEEE International Radar Conference 2016, Philadelphia, PA, USA.

Adriano Rosario Persico was born in Napoli, Italy, on October 7, 1988. He received his BSc and MSc from Università degli Studi di Napoli "Federico II", Italy, in 2011 and 2014, respectively, in Telecommunications Engineering. In 2018, he received the Ph.D. degree from the Department of

Electronic and Electrical Engineering, University of Strathclyde, Glasgow, UK. Focus of his PhD research was on new advanced signal processing methods and algorithms for space situation awareness and defence against airborne threats.

Currently he is a Research Assistant with CNIT, CNIT, viale G.P. Usberti, n. 181/A - 43124 Parma, c/o udr Università "Federico II", via Claudio 21, I-80125 Napoli, Italy, working on advanced radar signal processing algorithms for radar imaging by using passive bistatic radar in partnership with MBDA Italia, via Monte Flavio 45, Roma, Italy. His current research interests are in radar micro-Doppler, compressed sensing, MIMO system and space based radar design for multi target detection, localisation and recognition for space situation awareness.

Ian Proudler graduated from Oxford University in 1978 having read Physics. He spent two years doing R&D work in the electronics industry before obtaining a Ph.D. in Digital Signal Processing from Cambridge University in 1984.

He is currently a Professor of Signal Processing at Loughborough University. From 1986 until 2011 he worked in the Defence sector looking into various adaptive digital signal processing issues such as: numerical stability and efficient computation; antenna algorithm for HF communications; signal separation for ESM purposes; magnetic detection for maritime surveillance; and GPS anti-jam systems. He has published some 100+ research papers, contributed to four textbooks and holds a patent on an adaptive filtering architecture.

He was awarded the John Benjamin Memorial Prize, in 1992 and 2001, and the IEE J.J. Thomson Medal, in 2002, for his work on signal processing algorithms. He was an Honorary Editor for IEE Proceedings: Radar, Sonar and Navigation for ten years. He has been on the organising committee of several international conferences.

John J. Soraghan received the B.Eng. (Hons.) and M.Eng.Sc. degrees in electronic engineering from University College Dublin, Dublin, Ireland, in 1978 and 1983, respectively, and the Ph.D. degree in electronic engineering from the University of Southampton, Southampton, UK, in 1989. His doctoral research focused on synthetic aperture radar processing on the distributed array processor.

After graduation, he was with the Electricity Supply Board in Ireland and with Westinghouse Electric Corporation in the USA. In 1986, he joined the Department of Electronic and Electrical Engineering, University of Strathclyde, Glasgow, UK as a Lecturer. He was a Manager of the Scottish Transputer Centre from 1988 to 1991, Manager with the DTI Parallel Signal Processing Centre from 1991 to 1995, and the Head of the ICSP from 2005 to 2007. He became a Professor of signal processing in 2003 and has held the Texas Instruments Chair in Signal Processing since 2004. He is currently the Director of the Sensor Signal Processing Research Groups within the Centre for Signal and Image Processing, University of Strathclyde, Glasgow, U.K. His main research interests include signal processing theories, algorithms, with applications to radar, sonar, and acoustics, biomedical signal and image processing, video analytics, and condition monitoring.

Prof. Soraghan has supervised 45 researchers to Ph.D. graduation and has published more than 340 technical publications. He is a Member of the IET.

Alfonso Farina, LFIEEE, FIET, FREng, Fellow of EURASIP, received the degree in Electronic Engineering from the University of Rome (IT) in 1973. In 1974, he joined Selenia, then Selex ES, where he became Director of the Analysis of Integrated Systems Unit and subsequently Director of Engineering of the Large Business Systems Division. In 2012, he was Senior VP and Chief Technology Officer of the company, reporting directly to the President. From 2013 to 2014, he was senior advisor to the CTO. He retired in October 2014. From 1979 to 1985, he was also professor of "Radar Techniques" at the University of Naples (IT). He is the author of more than 700 peer-reviewed technical publications and of books and monographs (published worldwide), some of them also translated in to Russian and Chinese.

Some of the most significant awards he's received include: (2004) Leader of the team that won the First Prize of the first edition of the Finmeccanica Award for Innovation Technology, out of more than 330 submitted projects by the Companies of Finmeccanica 3 Group; (2005) International Fellow of the Royal Academy of Engineering, U.K., and the fellowship was presented to him by HRH Prince Philip, the Duke of Edinburgh; (2010) IEEE Dennis J. Picard Medal for Radar Technologies and Applications for "Continuous, Innovative, Theoretical, and Practical Contributions to Radar Systems and Adaptive Signal Processing Techniques"; (2012) Oscar Masi award for the AULOS® "green" radar by the Italian Industrial Research Association (AIRI); (2014) IET Achievement Medal for "Outstanding contributions to radar system design, signal, data and image processing, and data fusion". Distinguished Lecturer (DL) of IEEE AESS. (2017) IEEE SPS Industrial Leader Award for contributions to radar array processing and industrial leadership. (2018) The IEEE Signal Processing Society announced the 2018 Class of Distinguished Industry Lecturers for the term of 1 January 2018 to 31 December 2019.

Main received best paper awards: B. Carlton of IEEE – Trans. on AES (2001, 2003, 2013: assigned in 2018), IET – Proc. on Radar Sonar and Nav. (2009–2010) and Int. Conf. on Fusion (2004, 2009). He is a Visiting Professor at University College London (UCL), Dept. Electronic and Electrical Engineering and CTIF (Center for TeleInFrastructures) Industry Advisory Chair. He is consultant to Leonardo S.p.A. "Land and Naval Defence Electronics Division".